



**HAL**  
open science

## Effect of the solvent on the mechanical and structural properties of N-alkyldiamide organogels

Leïla Khacef, Philippe Legros, Pascal Hervé, Guillaume Ovarlez, Yaocihuatl Medina-Gonzalez

► **To cite this version:**

Leïla Khacef, Philippe Legros, Pascal Hervé, Guillaume Ovarlez, Yaocihuatl Medina-Gonzalez. Effect of the solvent on the mechanical and structural properties of N-alkyldiamide organogels. *Langmuir*, 2021, 37 (51), pp.14898-14910. 10.1021/acs.langmuir.1c02743 . hal-03798586v2

**HAL Id: hal-03798586**

**<https://hal.science/hal-03798586v2>**

Submitted on 5 Oct 2022

**HAL** is a multi-disciplinary open access archive for the deposit and dissemination of scientific research documents, whether they are published or not. The documents may come from teaching and research institutions in France or abroad, or from public or private research centers.

L'archive ouverte pluridisciplinaire **HAL**, est destinée au dépôt et à la diffusion de documents scientifiques de niveau recherche, publiés ou non, émanant des établissements d'enseignement et de recherche français ou étrangers, des laboratoires publics ou privés.

---

## Effect of the solvent on the mechanical and structural properties of N-alkyldiamide organogels

---

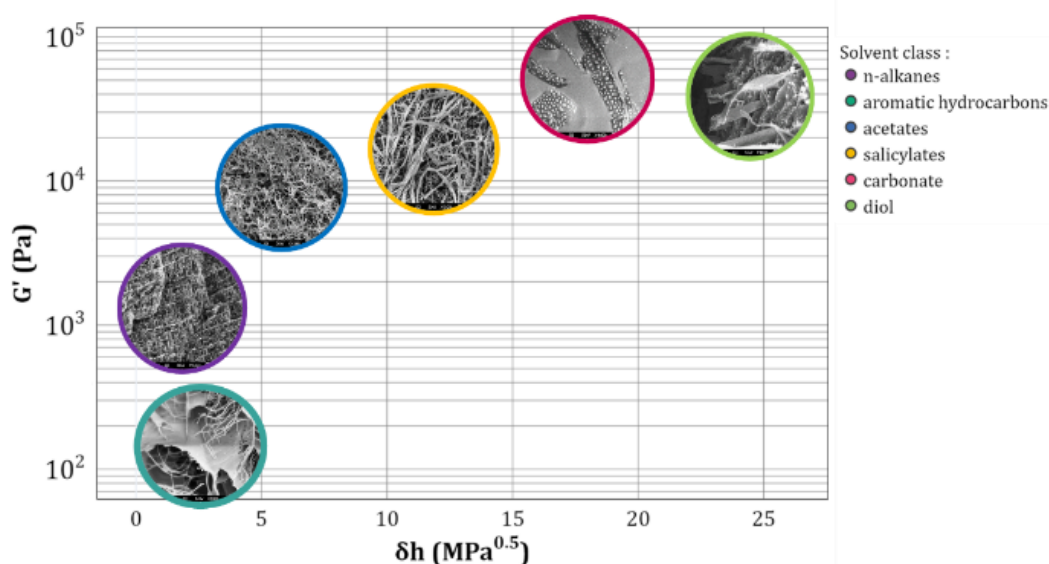
Leïla Khacef<sup>a,\*</sup>, Philippe Legros<sup>b</sup>, Pascal Hervé<sup>a</sup>, Guillaume Ovarlez<sup>a</sup> and Yaocihuatl Medina-Gonzalez<sup>a</sup>

<sup>a</sup>University of Bordeaux, CNRS, Solvay, LOF, UMR 5258, 33608 Pessac, France

<sup>b</sup>University of Bordeaux, CNRS, PLACAMAT, UMS3626, 33608 Pessac, France

\*Corresponding author. E-mail : leila.khacef-ext@solvay.com

### 1. Graphical abstract



### 2. Abstract

We study here organogels prepared thanks to a new organogelator, the N-oleyldiamide molecule which shows a remarkable propensity to gelify a large scope of solvents, from aprotic to high protic solvents. The solvent plays a key role in the formation and the stability of supramolecular self-assemblies. However the understanding and the control of its effects can be complex as many parameters are *a priori* involved. This study aims to understand the solvent effect on the organogels structures and on their final mechanical properties. Five solvent classes have been selected ranking from low protic to high protic, according to the Hansen H-bond parameter  $\delta h$ . The solvent proticity appears to be one of the main parameters that affects the organogel internal structure and therefore the final rheological properties. For a given organogelator fraction, the terminal elastic modulus measured by oscillatory rheology is observed to increase significantly with the Hansen H-bond solvent parameter  $\delta h$ . Materials of different mechanical properties are then shown to display various structures, which are investigated thanks to cryo-SEM. Besides, Wide-Angle X-ray Scattering (WAXS) has been used to probe the gelator organization at the molecular scale with regards to the solvent nature, in order to understand the supramolecular self-assembly of this promising molecule.

### 3. Introduction

Organogels are semi-solid materials composed of an organic solvent continuous phase trapped in a tridimensional network obtained by the self-assembly of low-molecular weight molecules called gelators<sup>1,2</sup>. Organogels systems are useful as rheological modifiers in the food industry (oleogels<sup>3-5</sup>), in biomedical applications<sup>6,7</sup> or in optoelectronic devices<sup>8-10</sup>. More generally, gel materials also encompass hydrogels, where the entrapped continuous phase is water. Hydrogels are well-described systems<sup>11,12</sup> and have a great interest in medical applications such as drug delivery and cell cultures due to their biocompatibility<sup>13,14</sup>. By contrast, organogels are less known and remain challenging materials because of the inherent nature of the solvent that present a broad spectrum of chemical structures. Nevertheless, the increasing amount of publications about organogels over the two past decades demonstrates the growing interest in the fundamental understanding of these materials. Indeed, most of the gelators have been discovered by serendipity and many try-and-error processes have been made as an attempt to design gelator molecules whose organogels display the required physico-chemical properties in one proper solvent. The organogel architecture is mainly anisotropic and can be attributed to physical forces such as electrostatic,  $\pi$ - $\pi$  stacking, Van der Waals or H-bonding interactions. The solvent is the key in mediating the aggregation and self-assembly of gelator molecules and determines the final type of organogel nanostructures (self-assembled fibrillar networks (SAFIN), rods, platelets etc...) that lead to a great variety of mechanical properties. Therefore, understanding the mechanisms relative to the solvent action is essential to predict the gelation behavior of a newly found gelator. Controlling the solvent effect is a complex task, as many solvents features are taking part into the self-assembly process. A significant effort has been devoted to understand and control solvent effects during gelation, for instance, multiscale relationships via computational methods that account for solvent physico-chemical properties and molecular conformations have been developed as well as predictive tools such as molecular dynamics, or machine learning.<sup>15,16</sup> Other solvent rationalization methods using solvent scales (for example solvatochromic solvent scales such as Kamlet-Taft and Catalan parameters) have been used to discriminate the pertinent interactions responsible for the gel formation.<sup>17-19</sup>

Here, the gelation of a new amide derivative gelator, the N-oleyldiamide molecule is presented. The aim of this work is to study the solvent effect on this organogelator. Thanks to a selection of appropriate solvents using Hansen solubility parameters as solvent descriptors, the correlation between mechanical properties of the obtained organogels and their respective microscopic structures with regards to the solvent nature is described.

### 4. Material and methods

#### a. Materials and sample preparation

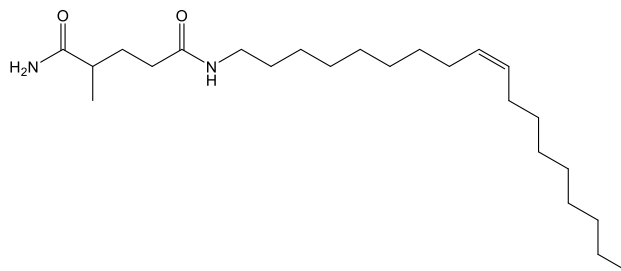


Figure 1: Gelator N-oleyldiamide (Gelator C18')

The gelator N-oleyldiamide (Figure 1), referred to as Gelator C18', has been synthesized by the Solvay Lyon Research & Innovation Center (RICL) according to methods presented in the patent

n° WO2017174615A1<sup>20</sup> and used without any modification. All of the solvents mentioned in this work were purchased from Sigma Aldrich with a purity from 98% to 99% and used as received. The gelification protocol is described as follows. The gelator C18' was weighted in a glass vial with a rubber-PTFE lined cap and the solvent was added. After sealing, the glass vial was placed in an oven at a temperature ranging between 110°C and 120°C (depending on the solvent boiling point) until complete solid dissolution was observed. The formulation was then let to cool down at room temperature and the gelification was assessed. For all of the organogels mentioned in this work, the gelator concentration was kept at 2 wt%, except for X-ray experiments where the organogels were formulated at 10 wt%, because of the sensibility limitations of the equipment.

#### b. Solvent description

- Hansen solubility parameters

From a macroscopic point of view, a solvent can be described by its bulk parameters such as dielectric constant, refractive index, partition coefficient, viscosity etc. However this description of the solvent as a macroscopic continuum may not be pertinent for understanding self-assembly processes where the formation of nanostructures result from the interplay between solvent and solute molecules. Indeed, at the vicinity of the solute molecules, solvent molecules can adopt different conformations to interact with the solute, changing the final packing of the solute molecules and therefore leading to different types of nanostructures. Those intermolecular solute-solvent interactions can be quantified by taking into account the solvent molecular properties, which may include H-bonding donor/acceptor, electrostatic or Van Der Waals interactions.<sup>18,19</sup> That is why, solvent scales such as Kamlet-Taft<sup>21</sup>, Catalan<sup>22</sup> and Hansen solubility parameters among others have been established in order to quantitatively describe those interactions. Indeed, solvent scales allow the decomposition of the solvent behavior into different contributions, which are useful in a first attempt to understand which solvent property is responsible for describing a phenomenon.

The Hansen Solubility Parameters (HSP)<sup>23</sup> are derived from the thermodynamics of solvation and the mean-field theory. The cohesive energy density (CED) of a molecule is the energy associated to its transition from a condensed state to a gas state. This energy, also known as the squared Hildebrand solubility parameter  $\delta$  is proportional to the heat of vaporization ( $\Delta E_v$ ) and is defined by (eq 1):

$$\delta^2 = \frac{\Delta E_v}{v_m} \quad (1)$$

$v_m$  is the molar volume of the molecule. As the Hildebrand parameter does not discriminate the intermolecular interactions due to polarity or H-bonding contribution, Hansen (1960) introduced the decomposition of this parameter into three contributions (eq 2):

$$\delta^2 = \delta d^2 + \delta p^2 + \delta h^2 \quad (2)$$

$\delta d$  is the dispersive contribution based on London Van Der Waals interactions. These interactions are predominant for aprotic and apolar molecules such as aliphatic and aromatic hydrocarbons.  $\delta p$  is the polar contribution (Keesom and Debye Van der Waals interactions). Finally,  $\delta h$  is the H-bonding contribution.

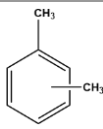
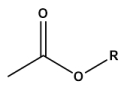
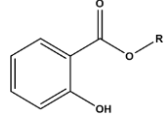
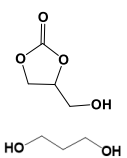
In the past years, Hansen solubility parameters have been extensively used for the prediction and comprehension of organogel formation. The Hansen parameters solvent database is available for a large number of solvents which makes it popular for industry. The three Hansen parameters of each solvent represent the solvent coordinates in a 3D space. As the Hansen theory is based on

“Like dissolves like”, the nearer two molecules are in this 3D space, the more likely they will dissolve each other. For an unknown compound of interest (usually polymers), solubility tests are performed using a large database of solvents. In the 3D space, the solvents leading to a solution form a solubility sphere. The distance between a solvent and the center of the sphere is relevant for describing the interaction between the two (soluble or insoluble). Based on a similar approach for organogels, Bouteiller et al<sup>24-26</sup> and Rogers et al<sup>27,28</sup>, have reported the use of the Hansen formalism to determine gelation spheres, by conducting gelification trials in a database of solvents. They have been able to make a link between the sphere features (coordinates and radius) and the gelator structural modification. The methodology adopted aimed to predict the gelation ability of new gelators based on the results from similar gelator molecules. In fine, the idea was to design gelator molecules with appropriate gelation properties. Other works<sup>29-31</sup>, have correlated the Hansen parameters of the solvents with some properties of the obtained organogels, such as mechanical properties (rheology) or gelification capability. In the present work, Hansen parameters have been used as solvent descriptors, which helped identifying interesting solvents for the study.

- Strategy for the solvent choice

First of all, gelification trials in a large database of 72 solvents have been conducted to identify relevant solvents for the study. The final formulations have been classified as solutions, precipitates and gels. Among the solvents leading to gels, five solvent groups have been selected which were sorted by proticity. First of all: n-alkanes; these solvents have been chosen because of their molecular structure simplicity (linear hydrocarbons) where only dispersion forces (Van Der Waals) take place. The second group of solvents were aromatic hydrocarbon solvents. These solvents display a small polarity contribution in comparison with the alkanes. The third group were acetates, which show H-bonding acceptor contribution related to the ester function. The fourth group were salicylates, beta-hydroxyesters, composed by an ester group (H-bond acceptor) and a hydroxyl group (H-bond donor). Finally, the last group of solvents gathered very protic solvents such as ethylene glycol (diol) and glycerol carbonate (carbonate). Some physicochemical properties of the solvents used in this study have been summarized in Table 1. The Hansen parameters (in MPa<sup>0.5</sup>) and the boiling points of the solvents have been taken from the HSPiP software<sup>32</sup>.

Table 1: HSP values and boiling points (Bp) of the selected solvents

Solvent class	Solvent	Generic structure	Bp (°C)	$\delta d$ (MPa <sup>0.5</sup> )	$\delta p$ (MPa <sup>0.5</sup> )	$\delta h$ (MPa <sup>0.5</sup> )
n-alkanes	Decane	$C_nH_{2n+2}$	174	15.7	0	0
	Dodecane		216	16	0	0
	Tetradecane		253	16.2	0	0
	Hexadecane		287	16.3	0	0
Aromatic hydrocarbons	o-xylene		144	17.8	1	3.1
	m-xylene		139	18.4	2.6	2.3
	Mesitylene		165	18	0.6	0.6
Acetates	Hexyl acetate		172	15.8	2.9	5.9
	Octyl acetate		211	15.8	2.9	5.1
	Decyl acetate		272	16.1	3.1	4
	Benzyl acetate		214	1.3	5.7	6
Salicylates	Methyl salicylate		220	18.1	8	13.9
	Ethyl salicylate		232	18.2	8.1	9.3
	Benzyl salicylate		318	19.1	8.2	11
Carbonate & Diol	Glycerol carbonate		137	17.9	25.5	17.4
	Ethylene glycol		197	17	11	26

### c. Rheological measurements

The rheological measurements were performed using a Netzsch Kinexus Ultra + rheometer, equipped with a temperature-controlled hood. The geometry used was a 40mm serrated parallel-plate geometry. The first rheological experiment consisted in measuring the gelification kinetics of the gel. After formulation, the sample was introduced into the rheometer with a gap fixed at 0.9 mm. Then, the gel was melted at around 120°C (depending on the solvent boiling point) and the material was sheared at 5 s<sup>-1</sup> during the process to ensure the homogeneous melting of the gel. This step was necessary to erase the sample history. The formulation was then cooled down at 10°C/min to 25°C. Throughout the cooling, an oscillatory measurement at 1 Hz with a 0.03% deformation was applied to monitor the evolution of the material viscoelastic properties. A normal force controlled (NFC)<sup>33</sup> protocol was used instead of a controlled gap protocol. The NFC protocol consists in measuring the normal force applied by the material on the rheometer at the liquid state (melt) and then implementing this value for the remaining sequence, when the material is gelled. This protocol ensures that the gel does not show any normal stress during the gelification, which could lead to its breakage. Moreover, it takes into account the possible syneresis that can occur over a long time of observation, which can lead to erroneous moduli values: the gap changes throughout the experiment to fit to the true gel volume at any time. The G' and G'' evolutions during cooling allowed to describe the gelification kinetics and the G' plateau value was determined after approximately 1h of experiment (depending on the sample). A shear strain amplitude sweep was then performed, by imposing at 1 Hz a strain ramp from 10<sup>-2</sup> % to 5.10<sup>2</sup> % of deformation (5 samples per decade). The end of the linear regime symbolized by the critical strain value ( $\gamma_c$ ), was determined as the strain where the G' value decreased by 5% as compared to the G' plateau value at low strain.

### d. Cryo-SEM analysis

The structural analysis of organogels is quite complex. The main difficulty comes from the fact that the internal structure of the organogels can be easily destroyed. Organogels are lyotropic systems that can undergo polymorphic phase transitions upon concentration change<sup>34-36</sup>. That is

why Scanning Electron Microscopy (SEM) was not a suitable technique as the solvent needs to be removed prior to the observation (leading to a xerogel). In order to keep intact the structure of the gel, cryo-SEM measurements were performed by using a JEOL High Resolution 6700F SEM. First of all, the organogel sample was cryogenized in vitrous nitrogen ( $-210^{\circ}\text{C}$ ,  $10^{-4}$  bar). As the freezing ramp was very fast (e.g.  $10^4$  K/s for water<sup>37</sup>), most of the solvents did not crystallize and stayed in the amorphous state (vitrification). This step ensured the immobilization of the fibrillar architecture. There is no generic rule to know which solvent can be vitrified or not, thus the propensity of a solvent to be vitrified had to be determined empirically<sup>37</sup>. The sample was then fractured in the microscope antechamber (allowing the direct observation of the sample) and the stage was heated up in order to obtain the solvent sublimation, which was characterized by a pressure increase in the antechamber from  $10^{-5}$  bar to  $10^{-2}$  bar. The sublimation depends on the thermodynamic properties of the solvent and the equations of state (such as Antoine's law) are not valid for these typical pressure and temperature ranges. Therefore, the sublimation temperatures cannot be predicted prior to the experiment and some solvents of the study could not be sublimated. Finally, the sample was metallized (Pd/Au) during 120s up to 240s depending on the sample, and the observation took place. Besides the gels observation, systematic cryo-SEM observation of the pure solvents was made to ensure that the objects seen in the gels were not crystallized solvent structures.

#### e. SAXS/WAXS

Wide-Angle X-ray Scattering (WAXS) experiments were performed on a XEUSS 2.0 device (XENOCs) with a microfocus copper anode source. Coupled to a FOX3D XENOCs single reflection optical mirror centered on the Cu K $\alpha$  radiation ( $\lambda = 1.54 \text{ \AA}$ ), the system delivers a 8KeV beam which is collimated and defined by a set of two motorized scatterless slits. The organogels at a concentration of 10 wt% were introduced in thin glass capillaries (1.5 mm of diameter) and exposed 3 hours. The data were collected by a two-dimensional DECTRIS PILATUS-300k placed at a distance of 338 mm giving access to scattering wavevector  $q$  values from 0.002 to  $1.14 \text{ \AA}^{-1}$ .

## 5. Results

### a. Rheological measurements

- Elastic modulus  $G'$

The strength of the gels was determined by studying the kinetics of gelification and measuring the elastic modulus  $G'$  at the end of the process. Each gel was monitored from its solution state to the gel state by measuring the evolution of the elastic and viscous moduli (respectively  $G'$  and  $G''$ ) during a quench. Before the sol-to-gel transition, the viscoelastic moduli were very difficult to measure. The sol-to-gel transition was characterized by a sharp increase of the  $G'$  value, rapidly becoming far larger than the  $G''$  value, which is typical of a solid-like viscoelastic material. Then the  $G'$  modulus tended to reach a plateau value after a few hours which indicated the end of the gelification process (Figure 2). This value can be referred to as the gel strength and it is a property that allows comparing the different gel behaviors. Depending on the solvent type, the plateau was reached at different times. It is also important to mention that these organogels are metastable materials that can display syneresis over time (gel contraction and solvent expulsion). Thus the experiment time had to be adjusted with regards to the gel stability timescale.

Correlation plots were made between the gel strength ( $G'$ ) of the gels and the different solvent parameters (macroscopic and microscopic parameters). Regarding the Hansen Solubility parameters (HSP), no trend was observed between  $G'$  and  $\delta d$  (Figure 3a). However, a correlation between  $G'$  and respectively the polarity  $\delta p$  and the proticity  $\delta h$  of the solvent was noticed (Figure

3b and Figure 3c). Indeed, the apolar/aprotic classes of solvents such as n-alkanes and aromatic hydrocarbons lead to weaker gels with a  $G'$  modulus between  $10^2$  and  $10^3$  Pa. When increasing the solvent polarity and proticity, the gels formed are stronger with a  $G'$  modulus as high as  $10^5$  Pa for very polar/protic solvents such as glycerol carbonate.

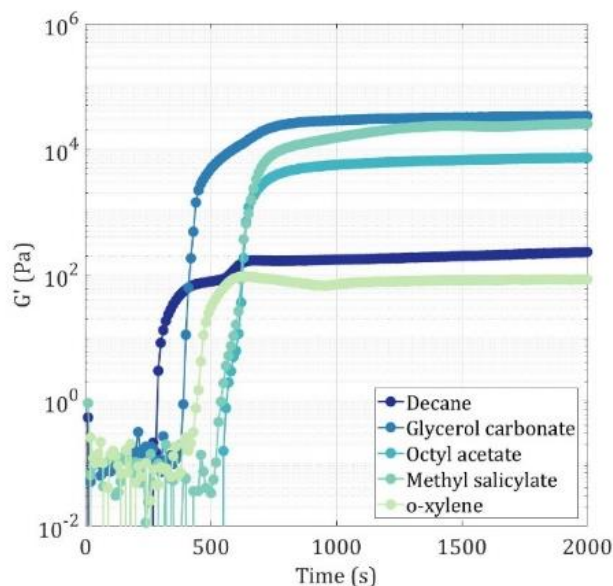


Figure 2 : Examples of gelification kinetics of the gelator C18' in decane, glycerol carbonate, octyl acetate, methyl salicylate and o-xylene

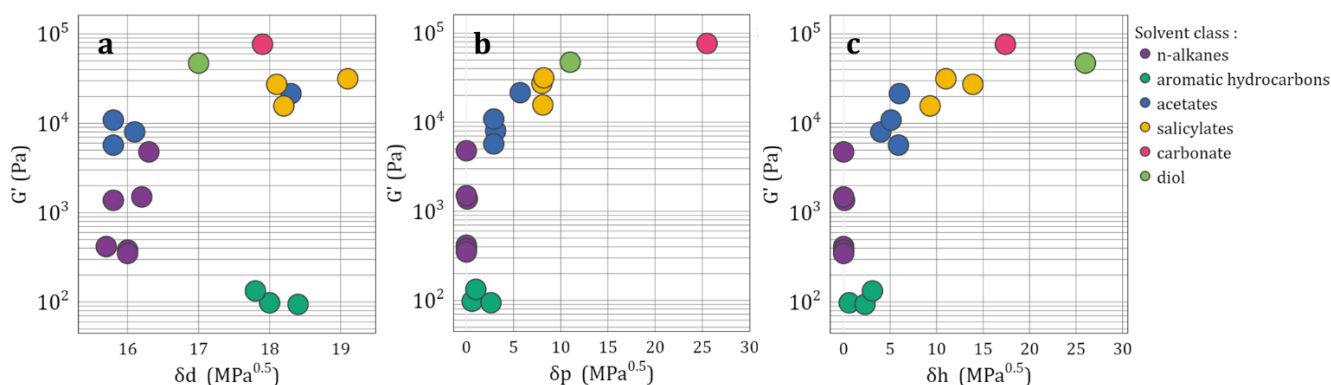


Figure 3 : Correlation plots between the elastic modulus of the organogels and the solvent HSP in different solvent classes

- Linear and non-linear regimes : Critical strain  $\gamma_c$ , plasticity and rupture

To have a better understanding of the gel viscoelastic properties, the linear domains of the materials were determined by performing a strain amplitude sweep experiment. At small values of deformation, the mechanical properties are independent of the applied strain (the linear viscoelastic region LVER). At a critical value of deformation (critical strain  $\gamma_c$  in %), the material starts to irreversibly deform, which is characterized by a decrease of the  $G'$  modulus. Then, the  $G'$  value decreases until crossing the value of  $G''$  and the system starts to flow (flow point). The amplitude sweep experiment allowed to access to two pieces of information: the critical strain and the rupture deformation profile (fragile or ductile). The Figure 4 shows the deformation profiles obtained for one gel of each solvent class. The dashed lines are a visual guide showing the ideal asymptotic behavior that a perfect ductile elastoplastic material



would have, namely a power law decay of power  $-3/2$  of  $G'$  as a function of strain<sup>38</sup>. The gels obtained in apolar solvents such as aromatic hydrocarbons and n-alkanes (Figure 4a: o-xylene and 4b: Dodecane for instance) displayed a long linear viscoelastic region (LVER) with a critical strain ranking between 1 and  $10^2$  %. At strain amplitudes larger than the critical strain, these materials underwent plastic transitions with a behavior close to an elastoplastic material, (power law decay of  $-3/2$ ). From a macroscopic point of view, these gels were “bouncy” and deformed easily (jelly-like materials). When the solvent proticity was increased (Figure 4c: Octyl acetate and 4d: Methyl salicylate for instance), the materials tended to have shorter LVER, and an abrupt drop of the  $G'$  modulus is observed at the moment of the fracture. This is consistent with the visual observation of the gels, these materials broke into pieces. For very protic solvents such as glycerol carbonate (Figure 4e), the gels showed very low critical strains ( $10^{-1}$  %). These gels had a more ductile rupture profile, with a smooth decrease of  $G'$ . These kinds of gels presented macroscopic turbidity and paste-like textures. Interestingly, the  $G'$  plateau values and the critical strain of the gels could be correlated (Figure 5). The gels with a higher elastic modulus are prone to deform irreversibly more easily upon deformation (short LVER). On the other hand, the gels that showed a good resistance towards deformation had a relatively low elastic modulus.

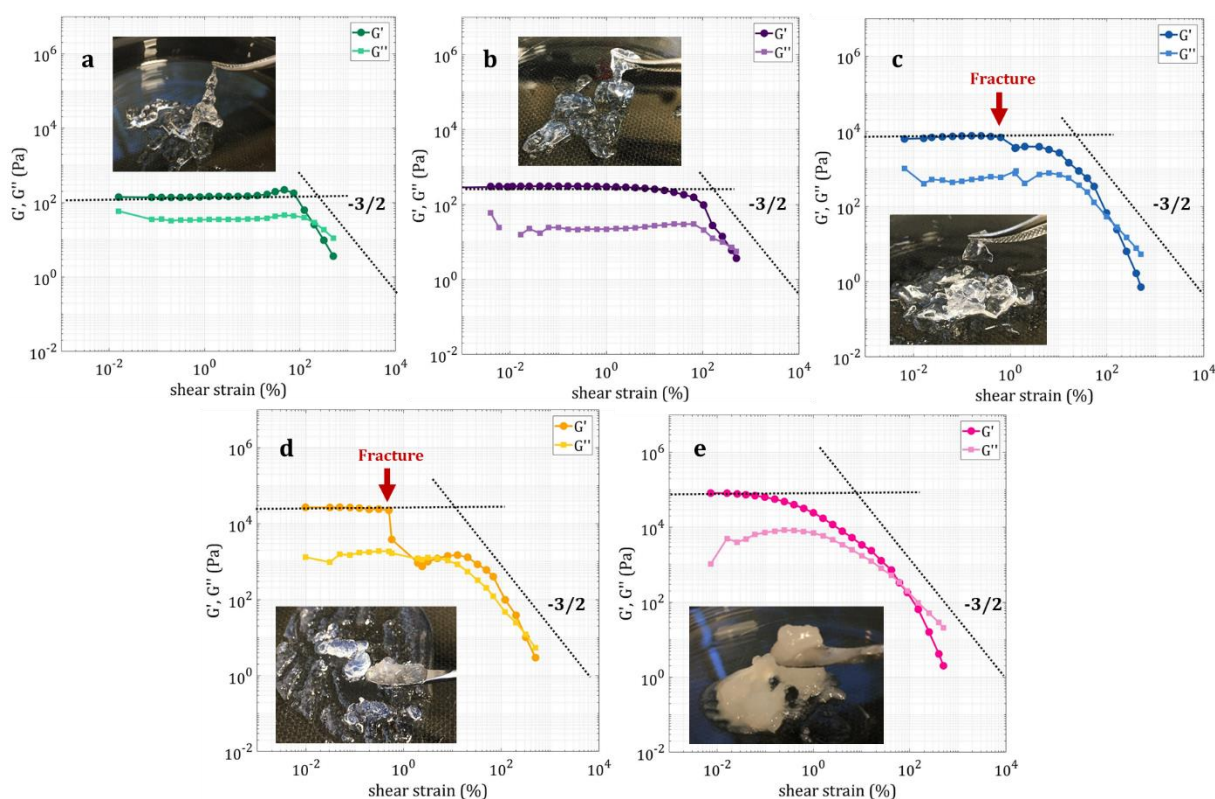


Figure 4: Shear strain sweep and visual aspect of the organogels (a. o-xylene gel, b. Dodecane gel, c. Octyl acetate gel, d. Methyl salicylate gel, e. Glycerol carbonate gel)

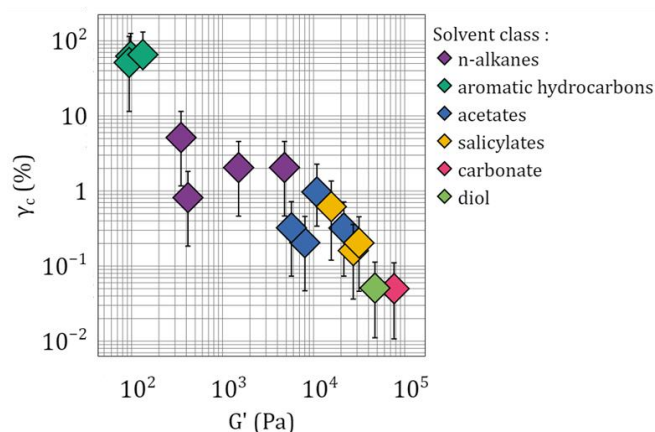


Figure 5: Correlation between the critical strain of the gels ( $\gamma_c$ ) and their respective elastic modulus ( $G'$ )

### b. Structural analysis of the organogels by cryo-SEM

Cryo-SEM experiments were performed on at least one solvent of each class, allowing to depict three different gel structures depending on the solvent type (proticity). The first group of solvents gathered the aromatics and n-alkanes, with o-xylene and dodecane gels as an example (Figure 6). These solvents can be designated as aprotic, with a very low or null H-bonding contribution. The corresponding organogels showed a fibrillar network where the fibrils seemed to be interconnected forming a long ordered pattern. Indeed, for the o-xylene gel, the structure was composed by tubes linked to each other like a honeycomb. The cells were probably made of bundles of fibrils agglomerated with some solvent that has not been sublimated. As the structure was very sensitive to the electron beam, the material composing the cell could not be fully investigated. Inside the cells, there were some fibrils with a diameter in the range between 30 and 70 nm. It is important to note that the size accuracy was highly dependent on the rate of solvent sublimation at the interface (fibril/solvent), therefore the size measurements were only used as a rough estimate. For the dodecane gel, the structure was well-organized and consisted in ridges spaced of about 1 $\mu$ m. Some fibrils of roughly 40 nm were making the junction between the ridges.

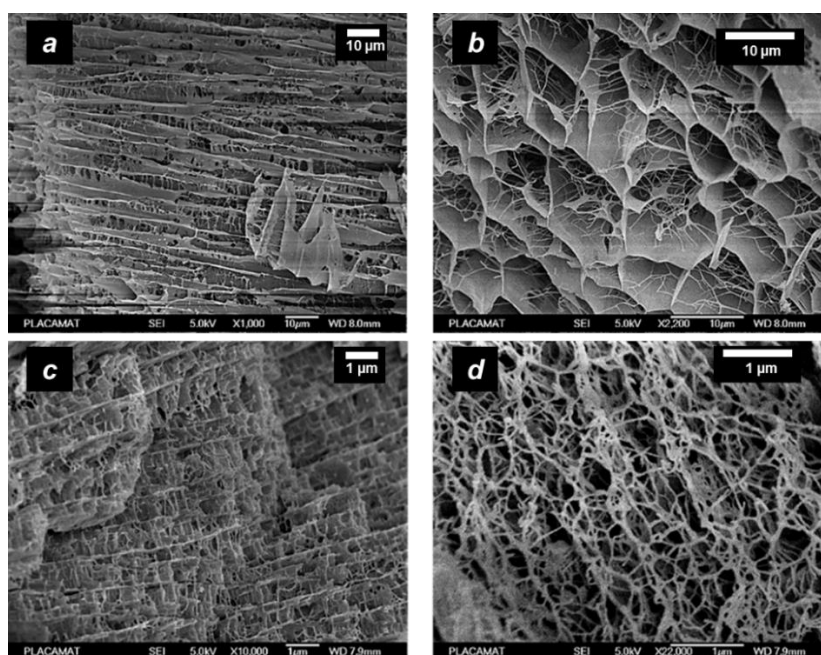


Figure 6: Cryo-SEM pictures of o-xylene gel (a, b) and dodecane gel (c, d)

The second group gathered the mid protic solvents (salicylates and acetates) with octyl acetate and methyl salicylate gels taken as an example (Figure 7). These gels did not present an apparent organization and were made of entangled fibrils. For the octyl acetate gel, the structure was composed of fibrils of an apparent diameter of approximately 70-80 nm. Interestingly, the methyl salicylate gel showed two populations of fibrils of different sizes: bundles of straight fibrils of around 200 nm diameter and thinner fibrils of around 75 nm diameter. The latter formed a network of entangled fibrils with a high number of junction points.

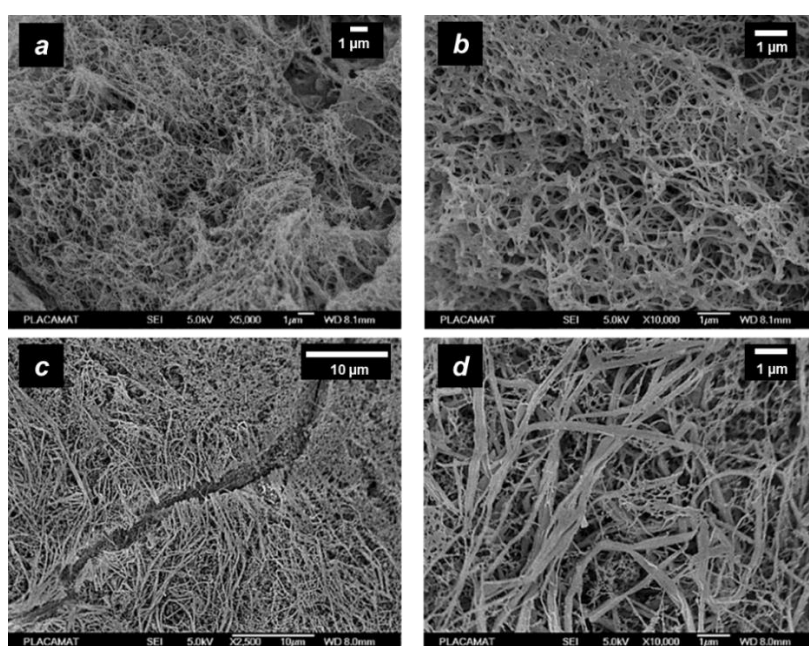


Figure 7: Cryo-SEM pictures of octyl acetate gel (a, b) and methyl salicylate gel (c, d)

With very protic solvents, different kinds of gels were observed. The third gel group gathered ethylene glycol and glycerol carbonate organogels (Figure 8). On a macroscopic scale, these gels were turbid and with a paste-like texture. On a microscopic scale, some short platelets of about 10-20 µm length and 1 µm width were observed. The platelets seemed to be in contact to each other but without any particular order. Indeed, during the solvent sublimation, the first layer of the material was taken away with the solvent suggesting that the connections between platelets were very weak, making impossible to reveal a long order organization without disrupting the network. Therefore the sizes given represent the sizes of the objects on the emergent part of the surface. Interestingly, the glycerol carbonate platelets showed some small droplets on the surface. We hypothesized that these droplets were composed of glycerol carbonate solvent which was not removed by sublimation.

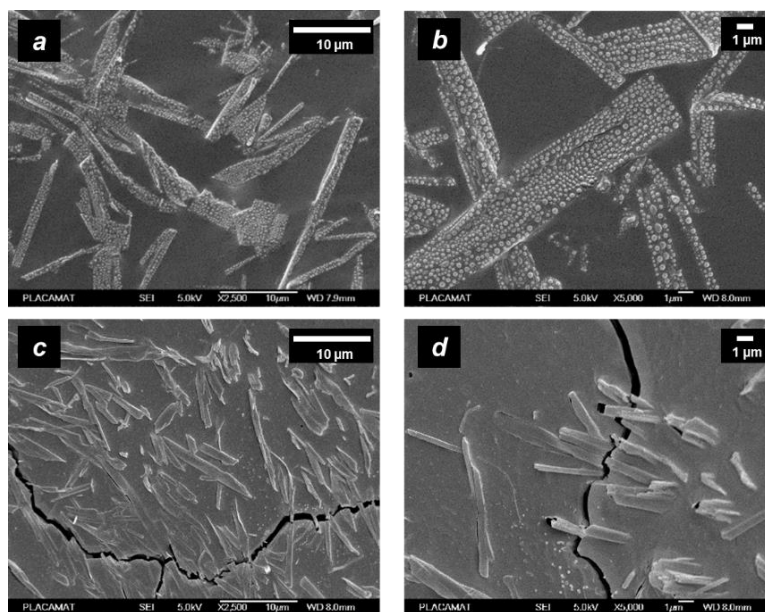


Figure 8: Cryo-SEM pictures of glycerol carbonate gel (a, b) and ethylene glycol gel (c, d)

### c. WAXS measurements

Wide Angle X-rays Scattering (WAXS) experiments have been made to probe the molecular organization of the nanostructures of the gelator C18' in the different solvent categories and to make a comparison with the solid form of the gelator. The  $q$ -region of interest was between 0.1 and  $0.7 \text{ \AA}^{-1}$  where the Bragg diffraction peaks could be observed. One gel of each solvent class has been studied. The different diffraction patterns of the gels and the gelator powder are shown in Figure 9. For the data analysis, all the pure solvent spectra have been systematically subtracted from the gel signal, except of *o*-xylene and methyl salicylate gels where the gel signals were too low compared to the solvent signal.

The gelator C18' crystalline powder exhibited distinct Bragg peaks in the ratio of 1;2;3;4 indicating a lamellar molecular organization<sup>39,40</sup>. Almost all the gels showed the same peaks except for the *o*-xylene gel, where a spread bump was observed. The peak indexations have been gathered in the Table 2, and the  $d$ -spacing values have been calculated by using the first-order diffraction peak. The gels obtained from alkane, acetate, salicylate and carbonate solvents showed similar crystalline packing arrangement as the powder. Therefore, in these solvents the gel fibers were exclusively crystalline. However, the results for *o*-xylene gel are completely different. The absence of crystalline peaks suggested that the gel fibers were amorphous<sup>41,42</sup>.

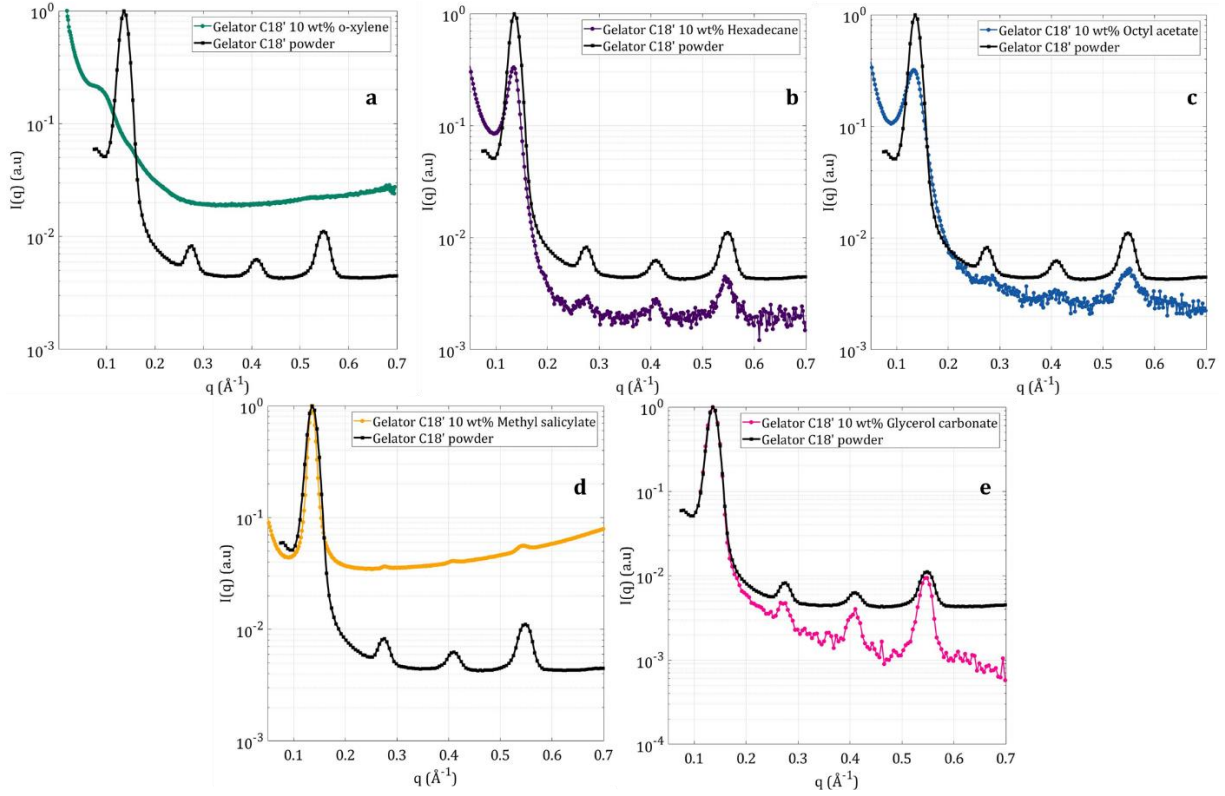


Figure 9: Comparison of WAXS profiles of the Gelator C18' crystalline powder and a. *o*-xylene gel, b. Hexadecane gel, c. Octyl acetate gel, d. Methyl salicylate gel and e. Glycerol carbonate gel.

Table 2: Bragg diffraction peak indexations and lamellar *d*-spacing (*d*) of C18' powder and corresponding gels in different solvents.

Sample	$q_1$ ( $\text{\AA}^{-1}$ )	$q_2$ ( $\text{\AA}^{-1}$ )	$q_3$ ( $\text{\AA}^{-1}$ )	$q_4$ ( $\text{\AA}^{-1}$ )	$d = \frac{2\pi}{q_1}$ ( $\text{\AA}$ )
C18' powder	0.1357	0.2757	0.4103	0.5485	46.3
C18' wt% Hexadecane	0.1345	0.2770	0.4105	0.5430	46.7
C18' 10 wt% Octyl acetate	0.1326	0.2855	0.4068	0.5517	47.4
C18' 10 wt% Methyl salicylate	0.1347	0.2753	0.4111	0.5438	46.6
C18' 10 wt% Glycerol carbonate	0.1357	0.2757	0.4103	0.5485	46.3

## 6. Discussion

### a. Organogel structure and mechanical properties relationship

The macroscopic properties of a heterogeneous material highly depend on the local mechanical properties and structure at various scales. Considering the observed fibrillary materials, we can expect their elastic modulus to depend on the individual fibril elastic modulus, on the fibril size, on the fibril volume fraction and on their spatial organization. The same gelator organization inside the fibrils (except for *o*-xylene gels) being provided by WAXS measurements, the fibril density should not be affected that much. Since we have compared materials of same gelator mass fraction in all solvents, the fibril volume fraction can therefore be considered as being the same in all of these materials. We thus need to understand which parameter among the fibril modulus, size and spatial organization, is likely to have the most important impact on the material macroscopic elastic modulus. The diameters of the fibrils have been calculated for all of the organogels studied by cryo-SEM and have been gathered in Table 3 along with the solvent  $\delta h$  parameter and the respective gel elastic modulus. We recall that the observed moduli vary by a factor  $10^3$  from  $10^2$  Pa in *o*-xylene to  $10^5$  Pa in glycerol carbonate. Regardless the type of gel

architecture, a correlation thus seemed to exist between the fibril diameter and the solvent proticity. High protic solvents enhanced the formation of coarser objects.

Table 3: Fibril diameters of the C18' organogels in the different solvents with regards to the gel elastic modulus ( $G'$ ) and the Hansen H-bond solvent parameter  $\delta h$ .

Solvent	$\delta h$ (MPa <sup>0.5</sup> )	Fibril diameter ( $\mu\text{m}$ )	$G'$ (Pa)
Dodecane	0	0.042	$3.10^2$
o-xylene	3.1	0.068	$1.10^2$
Octyl acetate	5.1	0.075	$3.10^4$
Methyl salicylate	13.9	0.075 / 0.2	$2.10^4$
Glycerol carbonate	17.4	1.0	$8.10^5$
Ethylene glycol	26	0.9	$5.10^5$

To better apprehend what can be expected for our gels, and see if a dependence on the fibril diameter makes sense, it is worth looking at the literature of similar loose structures that have been studied in-depth, e.g., low-density open-cell foams and cellulose fiber gels. For example, Warren and Kraynik<sup>43</sup> developed a micromechanical analysis of low-density foams with open cells, and showed that the elastic modulus of the bulk material is proportional to the ligament elastic modulus, and relies mostly on the ligament volume fraction. At a given volume fraction, however, the elastic modulus do not depend on the ligament size, and is not significantly modified with regards to the ligament geometry. It is noteworthy that only a limited size effect has been observed in nano-cellular foams, where the ligament internal structure starts to play a role (finite size effect)<sup>44</sup>. On the other hand, nanofibrillar dispersions such as cellulose nanofibrils<sup>45</sup> display, after the critical entanglement concentration, an increase of the elastic modulus with the fibril's aspect ratio or with decreasing fibril diameter, which is the opposite of our observation (materials of higher elastic moduli have the largest fibrils). In this perspective, the factor  $10^3$  observed for our materials seems to be possibly explained only if the various fibrils that are formed in the different solvents have very distinct intrinsic elastic moduli, or interfibrillar interactions; the observed variation of the fibril diameter would then be a side effect of a change in the fibril properties, but would not be directly at the origin of the elastic modulus increase.

Our materials showed a whole range of morphologies and mechanical properties, and the nature of the solvent was definitely accountable for these changes. For aprotic solvents such as n-alkanes and aromatics, cryo-SEM experiments of the corresponding gels showed a 3D fibrillar network with flexible fibrils self-aggregated into a long order organization, such as a honeycomb for o-xylene and ridges for dodecane gels. A well-organized structure prevented the material from easily breaking down under strain that is why these gels showed the highest values of critical strains. Besides of the long order structure, the apparent flexibility of the fibrils would imply that they have a small intrinsic elastic modulus which can explain the relative low elastic modulus  $G'$  values.

When increasing the solvent proticity (acetates and salicylates solvents) the well-organized structure of the gels was lost and it evolved to an entangled network of fibrils. Therefore the gels were expected to be less resistant towards strain. Indeed, the gels were more brittle which was indicated by a shorter linear viscoelastic region and a fragile rupture behavior. As no particular structure was observed, the entanglement points between fibrils in the network were not strong enough to keep the integrity of the network.

Finally, for very protic solvents such as ethylene glycol and glycerol carbonate, the gels consisted of a percolated network of straight platelets, which suggested that they were much stiffer than the previously observed fibrils, whose typical sizes were larger than those measured for the previous

fibrils. The apparent stiffness of the objects was consistent with a very high elastic modulus measured by rheology. The platelets did not seem to form a continuous network, but rather seemed to be in frictional contact. The material plasticity would then occur to slippage between platelets at their contact points, which would explain the low critical strain value of these gels.

### b. The solvent effect on the organogel self-assembly

The wide variety of mechanical properties observed in the organogels obtained with the gelator C18' was undoubtedly due to the nature of the solvent. The self-assembly phenomenon is a balance between gelator-gelator and solvent-gelator interactions. Strong gelator-gelator interactions lead to a precipitate while strong gelator-solvent interactions lead to solubilization. Changing the type of the solvent, changes the strength of these interactions, and thus the self-assembly process leading to different organogel structures with intrinsic mechanical properties. To understand the role of the solvent in the process, one has to consider the nature and the delicate balance of the interactions taking place for the gelator and the solvent molecules.

The gelator C18' molecule displayed two specific moieties where two kind of interactions could take place. First, there was the diamide group, which can self-assemble through H-bond interactions thanks to the primary amide. Then, the oleyl alkyl chain can provide additional Van Der Waals interactions and can strongly interact with the organic solvent (Figure 10). The WAXS experiments were useful to validate this possible scenario of self-assembly. Indeed, the WAXS results for the gelator crystalline powder exhibited a lamellar structure with a d-spacing of around 46 Å. Thanks to Chem3D and a MM2 force field minimization of the gelator molecule, we have calculated the length of one gelator molecule and the resulting dimer. We have obtained a dimer length of 42 Å, which was consistent with the WAXS results (46 Å). On the long range, the stacking of these molecules gave the final lamellar organization. (Figure 10)

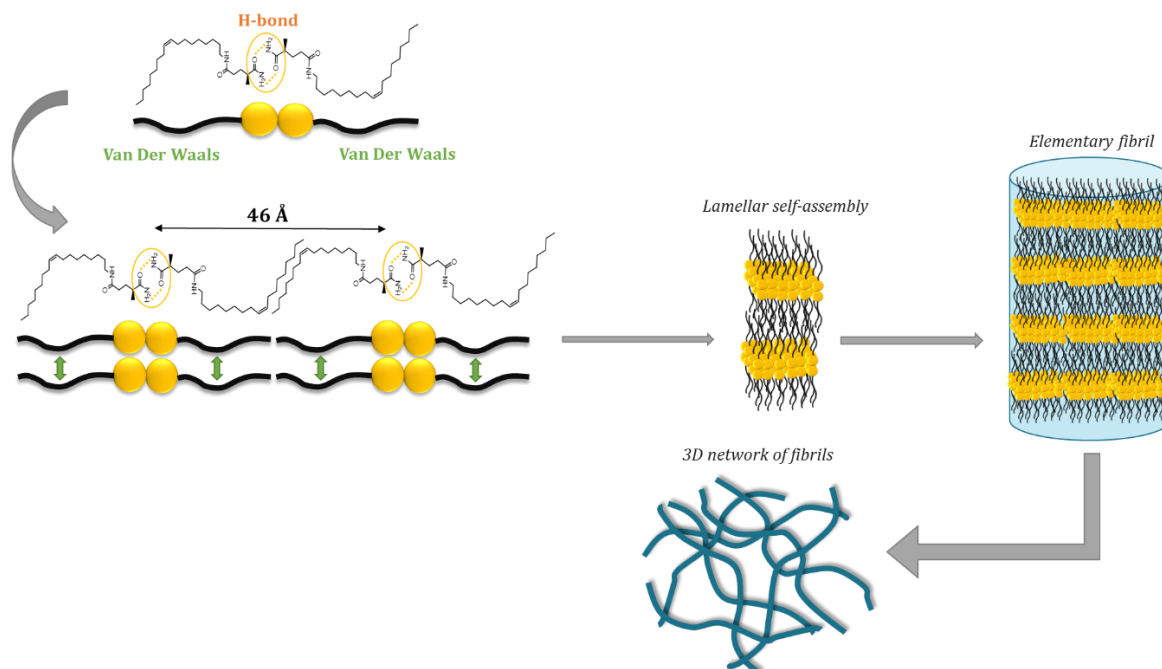


Figure 10: Schematic representation of the gelator C18' self-assembly through H-bonds and Van Der Waals interactions. The value of 46 Å corresponds to the value of the lamellar d-spacing of gelator C18' molecules from the WAXS experiment.

The solvents chosen for this study displayed different molecular structures, which can be accounted for the change in the solvent H-bonding Hansen parameter  $\delta_h$ . Overall, this parameter

is relevant for describing the different gel behaviors. However, for more precise studies concerning each solvent class, the molecular structure of the solvent needs to be considered.

Aprotic or low protic solvents such as n-alkanes and aromatics lead to transparent gels, suggesting that the objects formed were quite small and did not scatter the visible light. The microscopy images indicated a diameter in the range of 40 to 70 nm for the corresponding fibrils. Even though these solvents were classified in the same category, they showed different behaviors regarding the molecular self-assembly. Indeed, the WAXS results indicated different crystallinity for o-xylene and hexadecane gels. Regarding the possible solvent-gelator interactions, these two solvents could have interacted with the oleyl chain of the gelator molecule without disrupting the gelator H-bonding network through amides. In the case of n-alkanes, we hypothesized that the solvent molecules intercalated between the gelator alkyl chains to form a layered structure which was held together through attractive London interactions<sup>46,47</sup>. The lamellar long range self-assembly of the gelators was still maintained and not disrupted by the solvent molecules with the same arrangement as the crystalline powder, as shown by the diffraction pattern. Regarding o-xylene gel, the gelator molecules were in a disordered state, no diffraction pattern was observed so the gel was amorphous. Indeed, when o-xylene molecules entered between the oleyl gelator chains, a spatial rearrangement of the chains took place to accommodate the solvent molecules. We hypothesized that with aromatic solvents such as o-xylene, no attractive London interactions were present to reinforce the gelator oleyl chains arrangement and the system was not capable to produce a lamellar organization that is why those gels are classified as amorphous gels.

When the proticity of the solvent was increased, the solvent affinity with the gelator was changed. With mid-protic solvents such as salicylates and acetates, either the ester carbonyl (or the hydroxyl group of the salicylate molecule) could interact with the amide of the gelator thus disrupting the H-bonding gelator-gelator interactions, or the solvent molecules could only interact with each other. This last situation could lead to a precipitate. For the organogels formed with ester solvents, the microscopy showed an entangled fibrillar network, suggesting that the gelator's H-bonding interactions were still favorable. However, the fibrils were slightly bigger in size compared to aprotic solvent gels (80-200 nm) and from a macroscopic point of view, the gels were slightly turbid, which is a clue on the increase of crystallinity. Indeed, regarding the diffraction pattern of the corresponding gels, the salicylate and the acetate gels showed similar Bragg peaks to the powder, therefore a similar arrangement as in the crystalline gelator powder was obtained.

For very protic solvents, the gelator C18' behavior was relatively different depending on the solvent molecular structure. Surprisingly, aliphatic alcohols such as methanol ( $\delta h = 22.3 \text{ MPa}^{0.5}$ ), ethanol ( $\delta h = 19.4 \text{ MPa}^{0.5}$ ) or 1-butanol ( $\delta h = 15.8 \text{ MPa}^{0.5}$ ) completely dissolved the gelator. However, when the solvent class was changed from aliphatic alcohol to carbonate or diol solvents that display similar  $\delta h$  Hansen parameters (glycerol carbonate  $\delta h = 17.4 \text{ MPa}^{0.5}$  and ethylene glycol  $\delta h = 26 \text{ MPa}^{0.5}$ ), the gelator molecules aggregated into platelets (Figure 8). Therefore, the Hansen rationalization shows limitations when describing the entire process of gelification. The self-assembly process needs to be considered in terms of interactions between the relevant functional groups of both gelator and solvent molecules. Regarding glycerol carbonate or ethylene glycol gels, the bigger size of the aggregates (Figure 8, 1-10  $\mu\text{m}$ ) and the macroscopic turbidity suggested strong gelator-gelator interactions compared to solvent-gelator interactions. The gelator molecules tended to aggregate with each other in a closely packed network with an identical crystalline structure as the gelator powder (Figure 9e. and Table 2). We can have a clue on the gelator/solvent affinity thanks to cryo-SEM pictures of a glycerol carbonate gel (Figure 8a and 8b). The fibril surface showed droplets which we hypothesized to be glycerol carbonate remaining solvent. The appearance of such droplets during sublimation may demonstrate the bad



wetting of the solvent on the fibril surface, and therefore a low affinity between the solvent and the gelator's fibrils. Hence, the behavior of the gelator C18' in those high protic solvents was likely to be very close to a crystalline precipitate state, where the material was composed of a suspension of straight fibrils made of a crystallized organization of gelator C18' molecules.

## 7. Conclusion

The gelification of the N-oleyldiamide showed noteworthy results regarding the collection of a variety of solvents that can be gelified. Depending on the solvent proticity, the obtained gels exhibited distinct structural and rheological features. The important difference in elastic moduli can be attributed to an intrinsic property of each {solvent/gelator} system, but we hypothesized that most of the bulk elastic modulus change is accounted for the fibril individual elastic modulus change. Increasing the solvent proticity led to the formation of more brittle fibrils with a higher elastic modulus and a lower ability to be deformed. To understand these outcomes, one has to consider the delicate balance of interactions between the gelator and the solvent molecules. Indeed, WAXS experiments showed a typical lamellar arrangement of gelator molecules, based on H-bonding interactions between amide groups. Depending on the nature of the solvent, the solvent molecules can either disrupt this organization which will lead to amorphous gels (e.g. o-xylene gel), or strengthen the self-assembly by adding extra Van Der Waals forces (e.g. n-alkanes gels). For more protic solvents, the self-assembly of the gelator did not seem to be disturbed, thus the solvent molecules appeared to be rather interacting with each other than with the gelator molecules, that led to organogels getting closer to a crystalline precipitate state, and macroscopically paste-like materials (e.g. glycerol carbonate gel).

## References

- (1) Terech, P.; Weiss, R. G. Low Molecular Mass Gelators of Organic Liquids and the Properties of Their Gels. *Chem. Rev.* **1997**, *97* (8), 3133–3160. <https://doi.org/10.1021/cr9700282>.
- (2) George, M.; Weiss, R. G. Low Molecular-Mass Organic Gelators. In *Molecular Gels: Materials with Self-Assembled Fibrillar Networks*; Weiss, R. G., Terech, P., Eds.; Springer Netherlands: Dordrecht, **2006**; pp 449–551. [https://doi.org/10.1007/1-4020-3689-2\\_15](https://doi.org/10.1007/1-4020-3689-2_15).
- (3) Dassanayake, L. S. K.; Kodali, D. R.; Ueno, S. Formation of Oleogels Based on Edible Lipid Materials. *Curr. Opin. Colloid Interface Sci.* **2011**, *16* (5), 432–439. <https://doi.org/10.1016/j.cocis.2011.05.005>.
- (4) Marangoni, A. G.; Garti, N. An Overview of the Past, Present, and Future of Organogels. In *Edible Oleogels*; Elsevier, **2011**; pp 1–17. <https://doi.org/10.1016/B978-0-9830791-1-8.50004-8>.
- (5) Martins, A. J.; Vicente, A. A.; Pastrana, L. M.; Cerqueira, M. A. Oleogels for Development of Health-Promoting Food Products. *Food Sci. Hum. Wellness* **2020**, *9* (1), 31–39. <https://doi.org/10.1016/j.fshw.2019.12.001>.
- (6) Sahoo, S.; Kumar, N.; Bhattacharya, C.; Sagiri, S. S.; Jain, K.; Pal, K.; Ray, S. S.; Nayak, B. Organogels: Properties and Applications in Drug Delivery. *Des. Monomers Polym.* **2011**, *14* (2), 95–108. <https://doi.org/10.1163/138577211X555721>.
- (7) Esposito, C. L.; Kirilov, P.; Roullin, V. G. Organogels, Promising Drug Delivery Systems: An Update of State-of-the-Art and Recent Applications. *J. Controlled Release* **2018**, *271*, 1–20. <https://doi.org/10.1016/j.jconrel.2017.12.019>.
- (8) Rao, M. R.; Sun, S.-S. Supramolecular Assemblies of Amide-Derived Organogels Featuring Rigid  $\pi$ -Conjugated Phenylethynyl Frameworks. *Langmuir* **2013**, *29* (49), 15146–15158. <https://doi.org/10.1021/la402449e>.
- (9) Sugiyasu, K.; Fujita, N.; Shinkai, S. Fluorescent Organogels as Templates for Sol–Gel Transcription toward Creation of Optical Nanofibers. *J. Mater. Chem.* **2005**, *15* (27–28), 2747–2754. <https://doi.org/10.1039/B501067E>.
- (10) Ajayaghosh, A.; K. Praveen, V.; Vijayakumar, C. Organogels as Scaffolds for Excitation Energy Transfer and Light Harvesting. *Chem. Soc. Rev.* **2008**, *37* (1), 109–122. <https://doi.org/10.1039/B704456A>.
- (11) Akhtar, M. F.; Hanif, M.; Ranjha, N. M. Methods of Synthesis of Hydrogels ... A Review. *Saudi Pharm. J.* **2016**, *24* (5), 554–559. <https://doi.org/10.1016/j.jsps.2015.03.022>.
- (12) Laftah, W. A.; Hashim, S.; Ibrahim, A. N. Polymer Hydrogels: A Review. *Polym.-Plast. Technol. Eng.* **2011**, *50* (14), 1475–1486. <https://doi.org/10.1080/03602559.2011.593082>.
- (13) Caliari, S. R.; Burdick, J. A. A Practical Guide to Hydrogels for Cell Culture. *Nat. Methods* **2016**, *13* (5), 405–414. <https://doi.org/10.1038/nmeth.3839>.
- (14) Yang, L.; Zeng, Y.; Wu, H.; Zhou, C.; Tao, L. An Antioxidant Self-Healing Hydrogel for 3D Cell Cultures. *J. Mater. Chem. B* **2020**, *8* (7), 1383–1388. <https://doi.org/10.1039/C9TB02792K>.
- (15) Van Lommel, R.; De Borggraeve, W. M.; De Proft, F.; Alonso, M. Computational Tools to Rationalize and Predict the Self-Assembly Behavior of Supramolecular Gels. *Gels* **2021**, *7* (3), 87. <https://doi.org/10.3390/gels7030087>.
- (16) Ramos Sasselli, I.; Halling, P. J.; Ulijn, R. V.; Tuttle, T. Supramolecular Fibers in Gels Can Be at Thermodynamic Equilibrium: A Simple Packing Model Reveals Preferential Fibril Formation versus Crystallization. *ACS Nano* **2016**, *10* (2), 2661–2668. <https://doi.org/10.1021/acsnano.5b07690>.

- (17) Lan, Y.; G. Corradini, M.; G. Weiss, R.; R. Raghavan, S.; A. Rogers, M. To Gel or Not to Gel: Correlating Molecular Gelation with Solvent Parameters. *Chem. Soc. Rev.* **2015**, *44* (17), 6035–6058. <https://doi.org/10.1039/C5CS00136F>.
- (18) Kaszyńska, J.; Łapiński, A.; Bielejewski, M.; Luboradzki, R.; Tritt-Goc, J. On the Relation between the Solvent Parameters and the Physical Properties of Methyl-4,6-O-Benzylidene- $\alpha$ -d-Glucopyranoside Organogels. *Tetrahedron* **2012**, *68* (20), 3803–3810. <https://doi.org/10.1016/j.tet.2012.03.067>.
- (19) Wang, C.; Li, Z.; Wang, X.; Wei, W.; Chen, S.; Sui, Z. Gelation Mechanism and Microstructure of Organogels Formed with L-Valine Dihydrazide Derivatives. *Colloids Surf. Physicochem. Eng. Asp.* **2011**, *384* (1), 490–495. <https://doi.org/10.1016/j.colsurfa.2011.05.027>.
- (20) Jacquot, R.; Marion, P.; Herve, P.; BACK, O.; Sehgal, A. N-Alkyldiamide Compounds and Gels Comprising the Same. WO2017174615A1, October 12, **2017**.
- (21) Kamlet, M. J.; Abboud, J. L. M.; Abraham, M. H.; Taft, R. W. Linear Solvation Energy Relationships. 23. A Comprehensive Collection of the Solvatochromic Parameters, .Pi.\*, .Alpha., and .Beta., and Some Methods for Simplifying the Generalized Solvatochromic Equation. *J. Org. Chem.* **1983**, *48* (17), 2877–2887. <https://doi.org/10.1021/jo00165a018>.
- (22) Catalán, J. Toward a Generalized Treatment of the Solvent Effect Based on Four Empirical Scales: Dipolarity (SdP, a New Scale), Polarizability (SP), Acidity (SA), and Basicity (SB) of the Medium. *J. Phys. Chem. B* **2009**, *113* (17), 5951–5960. <https://doi.org/10.1021/jp8095727>.
- (23) *Hansen Solubility Parameters: A User's Handbook*, 2. ed.; Hansen, C. M., Ed.; CRC: Boca Raton, Fla, **2007**.
- (24) Bonnet, J.; Suissa, G.; Raynal, M.; Bouteiller, L. Organogel Formation Rationalized by Hansen Solubility Parameters: Dos and Don'ts. *Soft Matter* **2014**, *10* (18), 3154. <https://doi.org/10.1039/c4sm00244j>.
- (25) Nunes, D. R.; Raynal, M.; Isare, B.; Albouy, P.-A.; Bouteiller, L. Organogel Formation Rationalized by Hansen Solubility Parameters: Improved Methodology. *Soft Matter* **2018**, *14* (23), 4805–4809. <https://doi.org/10.1039/C8SM00562A>.
- (26) Bonnet, J.; Suissa, G.; Raynal, M.; Bouteiller, L. Organogel Formation Rationalized by Hansen Solubility Parameters: Influence of Gelator Structure. *Soft Matter* **2015**, *11* (11), 2308–2312. <https://doi.org/10.1039/C5SM00017C>.
- (27) Lan, Y.; Corradini, M. G.; Liu, X.; May, T. E.; Borondics, F.; Weiss, R. G.; Rogers, M. A. Comparing and Correlating Solubility Parameters Governing the Self-Assembly of Molecular Gels Using 1,3:2,4-Dibenzylidene Sorbitol as the Gelator. *Langmuir* **2014**, *30* (47), 14128–14142. <https://doi.org/10.1021/la5008389>.
- (28) Lan, Y.; Corradini, M. G.; Rogers, M. A. Do Molecular Gelators Cluster in Hansen Space? *Cryst. Growth Des.* **2014**, *14* (9), 4811–4818. <https://doi.org/10.1021/cg500985e>.
- (29) Liu, S.; Yu, W.; Zhou, C. Solvents Effects in the Formation and Viscoelasticity of DBS Organogels. *Soft Matter* **2013**, *9* (3), 864–874. <https://doi.org/10.1039/C2SM27030G>.
- (30) Xu, H.; Song, J.; Tian, T.; Feng, R. Estimation of Organogel Formation and Influence of Solvent Viscosity and Molecular Size on Gel Properties and Aggregate Structures. *Soft Matter* **2012**, *8* (12), 3478. <https://doi.org/10.1039/c2sm07387k>.
- (31) Diehn, K. K.; Oh, H.; Hashemipour, R.; Weiss, R. G.; Raghavan, S. R. Insights into Organogelation and Its Kinetics from Hansen Solubility Parameters. Toward a Priori Predictions of Molecular Gelation. *Soft Matter* **2014**, *10* (15), 2632. <https://doi.org/10.1039/c3sm52297k>.
- (32) Abbott, S.; Hansen, C. M. Hansen Solubility Parameters in Practice. **2015**, 269.

- (33) Mao, B.; Divoux, T.; Snabre, P. Normal Force Controlled Rheology Applied to Agar Gelation. *J. Rheol.* **2016**, *60* (3), 473–489. <https://doi.org/10.1122/1.4944994>.
- (34) Bai, B.; Li, Z.; Wang, H.; Li, M.; Ozaki, Y.; Wei, J. Exploring the Difference in Xerogels and Organogels through in Situ Observation. *R. Soc. Open Sci.* **2018**, *5* (1), 170492. <https://doi.org/10.1098/rsos.170492>.
- (35) Schwaller, D.; Zapién-Castillo, S.; Carvalho, A.; Combet, J.; Collin, D.; Jacomine, L.; Kékicheff, P.; Heinrich, B.; Lamps, J.-P.; Díaz-Zavala, N. P.; Mésini, P. J. Gel-to-Gel Non-Variant Transition of an Organogel Caused by Polymorphism from Nanotubes to Crystallites. *Soft Matter* **2021**, *17* (16), 4386–4394. <https://doi.org/10.1039/D1SM00195G>.
- (36) Sakurai, K.; Jeong, Y.; Koumoto, K.; Friggeri, A.; Gronwald, O.; Sakurai, S.; Okamoto, S.; Inoue, K.; Shinkai, S. Supramolecular Structure of a Sugar-Appended Organogelator Explored with Synchrotron X-Ray Small-Angle Scattering. *Langmuir* **2003**, *19* (20), 8211–8217. <https://doi.org/10.1021/la0346752>.
- (37) Cavalier, A.; Spehner, D.; Humbel, B. M. *Handbook of Cryo-Preparation Methods for Electron Microscopy*; CRC Press, **2008**; p 682.
- (38) Rouyer, F.; Cohen-Addad, S.; Höhler, R.; Sollich, P.; Fielding, S. M. The Large Amplitude Oscillatory Strain Response of Aqueous Foam: Strain Localization and Full Stress Fourier Spectrum. *Eur. Phys. J. E* **2008**, *27* (3), 309–321. <https://doi.org/10.1140/epje/i2008-10382-7>.
- (39) Martins, A. J.; Cerqueira, M. A.; Fasolin, L. H.; Cunha, R. L.; Vicente, A. A. Beeswax Organogels: Influence of Gelator Concentration and Oil Type in the Gelation Process. *Food Res. Int.* **2016**, *84*, 170–179. <https://doi.org/10.1016/j.foodres.2016.03.035>.
- (40) Cerqueira, M. A.; Fasolin, L. H.; Picone, C. S. F.; Pastrana, L. M.; Cunha, R. L.; Vicente, A. A. Structural and Mechanical Properties of Organogels: Role of Oil and Gelator Molecular Structure. *Food Res. Int.* **2017**, *96*, 161–170. <https://doi.org/10.1016/j.foodres.2017.03.021>.
- (41) Jeong, Y.; Hanabusa, K.; Masunaga, H.; Akiba, I.; Miyoshi, K.; Sakurai, S.; Sakurai, K. Solvent/Gelator Interactions and Supramolecular Structure of Gel Fibers in Cyclic Bis-Urea/Primary Alcohol Organogels. *Langmuir* **2005**, *21* (2), 586–594. <https://doi.org/10.1021/la047538t>.
- (42) Takeno, H. Synchrotron Small-Angle X-Ray Scattering and Small-Angle Neutron Scattering Studies of Nanomaterials. In *X-ray and Neutron Techniques for Nanomaterials Characterization*; Kumar, C. S. S. R., Ed.; Springer Berlin Heidelberg: Berlin, Heidelberg, **2016**; pp 717–760. [https://doi.org/10.1007/978-3-662-48606-1\\_13](https://doi.org/10.1007/978-3-662-48606-1_13).
- (43) Warren, W. E.; Kraynik, A. M. Linear Elastic Behavior of a Low-Density Kelvin Foam With Open Cells. *J. Appl. Mech.* **1997**, *64* (4), 787–794. <https://doi.org/10.1115/1.2788983>.
- (44) Hodge, A. M.; Biener, J.; Hayes, J. R.; Bythrow, P. M.; Volkert, C. A.; Hamza, A. V. Scaling Equation for Yield Strength of Nanoporous Open-Cell Foams. *Acta Mater.* **2007**, *55* (4), 1343–1349. <https://doi.org/10.1016/j.actamat.2006.09.038>.
- (45) Cinar Ciftci, G.; Larsson, P. A.; Riazanova, A. V.; Øvrebø, H. H.; Wågberg, L.; Berglund, L. A. Tailoring of Rheological Properties and Structural Polydispersity Effects in Microfibrillated Cellulose Suspensions. *Cellulose* **2020**, *27* (16), 9227–9241. <https://doi.org/10.1007/s10570-020-03438-6>.
- (46) Giese, M.; Albrecht, M. Alkyl-Alkyl Interactions in the Periphery of Supramolecular Entities: From the Evaluation of Weak Forces to Applications. *ChemPlusChem* **2020**, *85* (4), 715–724. <https://doi.org/10.1002/cplu.202000077>.

- (47) Danovich, D.; Shaik, S.; Neese, F.; Echeverría, J.; Aullón, G.; Alvarez, S. Understanding the Nature of the CH $\cdots$ HC Interactions in Alkanes. *J. Chem. Theory Comput.* **2013**, 9 (4), 1977–1991. <https://doi.org/10.1021/ct400070j>.